

Sequential Kibble-Zurek dynamics in the anisotropic Ising model of the Si(001) surface

G. Schaller,¹ F. Queisser,¹ S.P. Katoorani,¹ C. Brand,² C. Kohlfürst,¹ M.R. Freeman,³
A. Hucht,² P. Kratzer,² B. Sothmann,² M. Horn-von Hoegen,² and R. Schützhold^{1,4}

¹*Helmholtz-Zentrum Dresden-Rossendorf, Bautzner Landstraße 400, 01328 Dresden, Germany,*

²*Fakultät für Physik, Universität Duisburg-Essen, Lotharstraße 1, 47057 Duisburg, Germany,*

³*Department of Physics, University of Alberta, 4-181 Centennial Center
for Interdisciplinary Science Edmonton, Alberta T6G 2E1, Canada,*

⁴*Institut für Theoretische Physik, Technische Universität Dresden, 01062 Dresden, Germany,*

(Dated: October 30, 2023)

As a simplified description of the non-equilibrium dynamics of buckled dimers on the Si(001) surface, we consider the anisotropic 2D Ising model and study the freezing of spatial correlations during a cooling quench across the critical point. The dependence of the frozen correlation lengths ξ_{\parallel} and ξ_{\perp} on the cooling rate obtained numerically matches the Kibble-Zurek scaling quite well. However, we also find that the ratio $\xi_{\parallel}/\xi_{\perp}$ of their frozen values deviates significantly from the ratio in equilibrium. Supported by analytical arguments, we explain this difference by the fact that the deviation from equilibrium in the weakly coupled direction occurs earlier than in the strongly coupled direction.

Introduction Von Neumann once [1] compared non-equilibrium theory to a theory of non-elephants – indicating the richness and complexity of this field, which we are just beginning to understand. In view of the diverging response time near the critical point, continuous phase transitions are prototypical candidates for observing non-equilibrium behavior [2, 3]. A prominent example is the Kibble mechanism describing the formation of topological defects during symmetry-breaking phase transitions in the early universe [4]. Later Zurek realized that quite analogous effects should also occur in condensed matter such as superfluid helium [5]. The Kibble-Zurek mechanism has been studied in numerous theoretical (e.g. [6–15]) and experimental investigations (e.g. [16–21]). An important point is the transition from adiabatic evolution to non-equilibrium behavior (such as freezing) when approaching or traversing the critical point. Apart from the original idea of creating topological defects, the general mechanism can also be applied to the frozen domain structure in symmetry-breaking phase transitions induced by the critical slowing down.

In the following, we shall study the anisotropic Ising model in two spatial dimensions [22–27] with special emphasis on possible differences in the non-equilibrium behavior between the two directions. Apart from advancing our fundamental understanding, these investigations are also motivated by the fact that the buckling dynamics of dimers on the Si(001) surface can be described by the anisotropic 2D Ising model [28–37]. Here, we consider the transition from the $p(2 \times 1)$ to the $c(4 \times 2)$ reconstruction at a critical temperature $T_{\text{crit}} \approx 190$ K. Since the (001) face of single-crystalline silicon belongs to the most important surfaces both in technology and science, our results will also be relevant in this regard. For example, the dependence of the frozen domain structure on the cooling rate indicates how sufficiently homogeneous Si(001) surfaces should be prepared.

Kibble-Zurek scaling Let us briefly recapitulate the main arguments leading to the standard Kibble-Zurek scaling. We consider a symmetry-breaking second-order phase transition at the critical temperature T_{crit} . Approaching the critical point T_{crit} , the equilibrium correlation length ξ^{eq} obeys the universal scaling behavior

$$\xi^{\text{eq}} \sim \left| \frac{T - T_{\text{crit}}}{T_{\text{crit}}} \right|^{-\nu} \equiv |\tau|^{-\nu} \quad (1)$$

with the universal critical exponent ν and the dimensionless reduced temperature τ . Similarly, the response or relaxation time $t_{\text{relax}}^{\text{eq}}$ (in equilibrium) scales as

$$t_{\text{relax}}^{\text{eq}} \sim |\tau|^{-z\nu} \sim (\xi^{\text{eq}})^z \quad (2)$$

with the dynamical critical exponent z . The divergence of $t_{\text{relax}}^{\text{eq}}$ at the critical point is the hallmark of critical slowing down.

Now the idea is to infer non-equilibrium properties from these equilibrium values. Let us assume a linear time-dependence for the cooling protocol $\tau(t) = -\eta t$ with the cooling rate η such that, starting at the time $t_{\text{in}} < 0$, the critical point is reached at $t = 0$. Then we may estimate the freezing time via $|t_{\text{freeze}}| = t_{\text{relax}}^{\text{eq}}(\tau_{\text{freeze}})$ where $\tau_{\text{freeze}} = \tau(t_{\text{freeze}})$, after which the system has no time to equilibrate any more. Insertion into Eq. (2) yields $|t_{\text{freeze}}| \sim \eta^{-z\nu/(z\nu+1)}$ and thus we obtain the frozen correlation length from Eq. (1)

$$\xi_{\text{freeze}} = \xi^{\text{eq}}(\tau_{\text{freeze}}) \sim \eta^{-\nu/(z\nu+1)}, \quad (3)$$

which is referred to as Kibble-Zurek scaling [9, 16, 20].

Anisotropic Ising model Now let us apply these ideas to the non-equilibrium dynamics of buckled dimers on the Si(001) surface which form a rectangular lattice. If we describe the tilt of the dimer at lattice site $i, j \in \mathbb{Z}$ to the left or the right by the pseudo-spin variable $\sigma_{i,j} = +1$ or $\sigma_{i,j} = -1$, respectively, the resulting energy landscape

corresponds to the anisotropic Ising model [28–30, 32–35].

$$E_{\sigma} = -J_x \sum_{i,j} \sigma_{i,j} \sigma_{i+1,j} - J_y \sum_{i,j} \sigma_{i,j} \sigma_{i,j+1} - J_{\times} \sum_{i,j} \sigma_{i,j} [\sigma_{i+1,j+1} + \sigma_{i+1,j-1}] \quad (4)$$

with a strong anti-ferromagnetic coupling $J_x \approx -25$ meV in x -direction (i.e., along the dimer rows) and weaker couplings $J_y \approx 3.2$ meV in y -direction (i.e., across the rows) as well as in diagonal direction $J_{\times} \approx 2.0$ meV [36, 37]. The latter two can be combined into an effective transversal coupling $J_{\perp} = J_y - 2J_{\times} \approx -0.8$ meV. As a result, the Ising model (4) favors anti-ferromagnetic order both in x - and y -direction. For convenience, we apply a checker-board transformation $\sigma_{i,j} \rightarrow (-1)^{i+j} \sigma_{i,j}$ after which we have ferromagnetic order since J_x and J_y change sign.

As explained above, the Kibble-Zurek scaling is derived from the equilibrium properties. For the Ising model (4), they can be obtained by Onsager theory [38]. In terms of the longitudinal $J_{\parallel} = J_x$ and transversal J_{\perp} couplings, the critical temperature $T_{\text{crit}} = 1/(k_B \beta_{\text{crit}})$ is determined by the relation $\sinh(2\beta_{\text{crit}} J_{\parallel}) \sinh(2\beta_{\text{crit}} J_{\perp}) = 1$. Thus, in the limit of strong anisotropy $J_{\parallel} \gg J_{\perp}$, we obtain the hierarchy of scales $J_{\parallel} \gg \beta_{\text{crit}}^{-1} \gg J_{\perp}$. Approaching the critical point from above, the correlation lengths ξ_{\parallel} and ξ_{\perp} in x - and y -direction (i.e., along the dimer rows and perpendicular to them) both obey the scaling (1) with the critical exponent $\nu = 1$, though with different prefactors [22, 24]. Thus, their ratio stays constant and is given by $\xi_{\perp}/\xi_{\parallel} = \sinh(2\beta_{\text{crit}} J_{\perp}) \approx 2\beta_{\text{crit}} J_{\perp}$.

Rate equations For the 2D Ising model, the dynamical critical exponent reads $z = 2 + \varepsilon$ where ε is a small and positive number [39–45]. Thus, the exponent in the Kibble-Zurek scaling relation (3) is roughly minus one third.

To test this relation, we have to study the non-equilibrium dynamics of the Ising model (4). To this end, we employ rate equations for the probabilities P_{σ} of the configurations σ in the standard form

$$\dot{P}_{\sigma} = \sum_{\sigma'} [R_{\sigma' \rightarrow \sigma} P_{\sigma'} - R_{\sigma \rightarrow \sigma'} P_{\sigma}]. \quad (5)$$

Neglecting correlated flips of two or more pseudo-spins (i.e., dimers), we use single-flip transition rates

$$R_{\sigma' \rightarrow \sigma} = \frac{\Gamma \exp\{-\beta E_B\}}{\exp\{\beta(E_{\sigma} - E_{\sigma'})\} + 1}. \quad (6)$$

The “knocking” frequency $\Gamma \approx 10^{12}$ /s and Arrhenius barrier height $E_B \approx 100$ meV are obtained from microscopic considerations [37, 46, 47]. The Glauber factor in the denominator can also be motivated by microscopic models, e.g., in the form of a reservoir of two-level systems or via

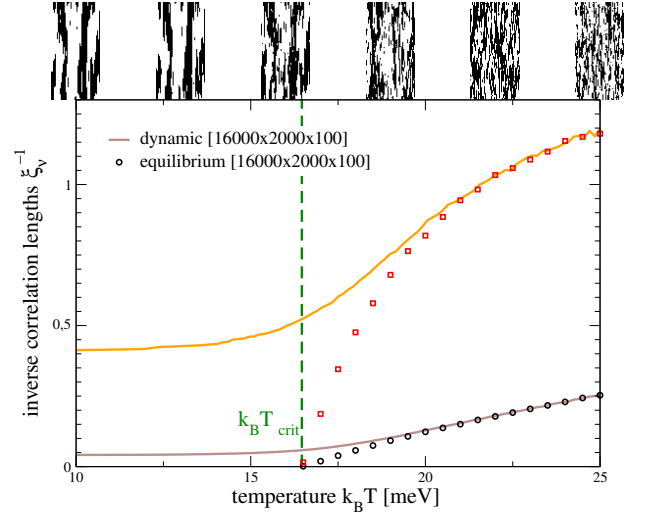


FIG. 1. Plot of inverse correlation lengths versus temperature (or, equivalently, time) for a cooling sweep for a 16000×2000 lattice, averaged over 100 trajectories. The correlation length in weakly-coupled direction (yellow curve) departs earlier than the other (brown curve) from the equilibrium solutions (red squares and black circles). On top, we added snap-shots of the time evolution of an example configuration at the respective temperatures as an illustration.

fermionic tunneling. It ensures that the rate is bounded $R_{\sigma' \rightarrow \sigma} < \Gamma \exp\{-\beta E_B\}$ and satisfies the detailed balance condition $R_{\sigma' \rightarrow \sigma}/R_{\sigma \rightarrow \sigma'} = \exp\{\beta(E_{\sigma} - E_{\sigma'})\}$ which enforces convergence to thermal equilibrium for constant parameters Γ and β etc.

Numerical simulations Due to the exponential dimensionality of (5) for an $N_x \times N_y$ spin lattice, we calculate trajectory solutions. For a given configuration σ , we propagate time by the stochastic waiting time τ_{σ} found by numerically solving $\ln(1 - r) = -\sum_{\sigma'} \int_t^{t+\tau_{\sigma}} R_{\sigma \rightarrow \sigma'}(t') dt'$, with uniformly distributed random number $r \in [0, 1]$, and perform a jump to a different state with the conditional probability [48, 49] given by $P_{\sigma \rightarrow \sigma'} = R_{\sigma \rightarrow \sigma'} / [\sum_{\sigma'' \neq \sigma} R_{\sigma \rightarrow \sigma''}]$. In the selection of jumps, we take advantage [50] of the fact that the $N_x N_y$ different single-spin flip processes can be grouped into 45 classes with identical energy differences entering the rates (6). Eventually, denoting the fast Fourier transformed spin lattice by $\tilde{\sigma}_{k_x k_y}$, the correlation lengths ξ_{\parallel} and ξ_{\perp} are then given by the inverse widths of the one-dimensional lattices $\sum_{k_y} |\tilde{\sigma}_{k_x k_y}|^2$ and $\sum_{k_x} |\tilde{\sigma}_{k_x k_y}|^2$, respectively. Averaging over multiple trajectories (and the resulting $|\tilde{\sigma}_{k_x k_y}|^2$) can be used to improve the statistics.

In Fig. 1, we contrast the time-dependent averaged correlation lengths (solid curves) with equilibrium versions (symbols) for a cooling sweep. Already at temperatures above T_{crit} , the correlation lengths depart from their equilibrium limits, but furthermore we see that this happens earlier for the weakly coupled direction.

The final (i.e., frozen) correlation lengths are depicted

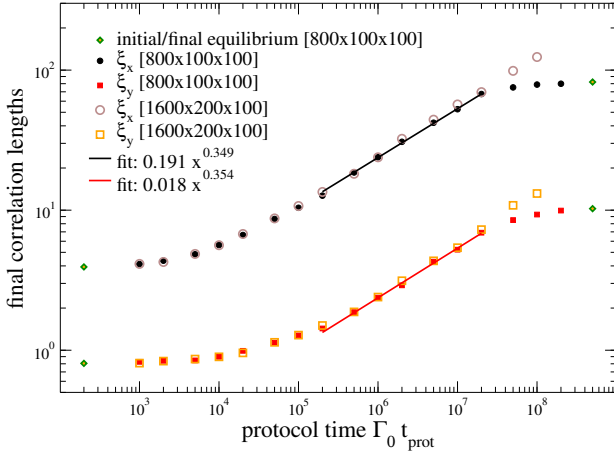


FIG. 2. Plot of the final (frozen) correlation lengths for different lattice sizes and averaged over 100 trajectories $[N_x \times N_y \times N_{\text{trj}}]$ for different cooling sweeps, where the system is cooled down from $k_B T_{\text{in}} = 25$ meV to $k_B T_{\text{out}} = 10$ meV (as in Fig. 1) in various time intervals, i.e., protocol times t_{prot} . For too fast protocols (left), the system can never follow, but Kibble-Zurek scaling is recovered for intermediate protocol times. Finite-size effects are visible for slow protocols.

in Fig. 2 as a function of the cooling rate $\eta \propto 1/t_{\text{prot}}$. For very fast sweeps, the system cannot follow and basically remains at the initial equilibrium values. For intermediate-speed sweeps, we find that both final correlation lengths follow a universal power-law increase, consistent with the Kibble-Zurek exponent $\nu/(1+z\nu) \approx 1/3$ in Eq. (3), see the fitted regions in Fig. 2. For very slow sweeps, we find that finite-size effects start to play a role.

Again, since the frozen correlation lengths $\xi_{\parallel}^{\text{freeze}}$ and $\xi_{\perp}^{\text{freeze}}$ both obey the scaling (3) in this intermediate region, though with different pre-factors, their ratio $\xi_{\perp}^{\text{freeze}}/\xi_{\parallel}^{\text{freeze}}$ is roughly constant – similar to the equilibrium case discussed above where $\xi_{\perp}^{\text{eq}}/\xi_{\parallel}^{\text{eq}} = \sinh(2\beta_{\text{crit}} J_{\perp}) \approx 2\beta_{\text{crit}} J_{\perp}$. However, we find that these two ratios are not the same, but differ by roughly a factor of two.

1D Ising model In order to understand the difference between the strongly and the weakly coupled directions found above, let us first consider the limiting case $J_y \rightarrow 0$ and $J_x \rightarrow 0$ of the 2D Ising model (4) where each row j separately forms a 1D Ising model with $J = J_x$

$$E_{\sigma}^{1D} = -J \sum_i \sigma_i \sigma_{i+1}. \quad (7)$$

Assuming translational invariance, we may derive an exact evolution equation for the correlator $c_a = \langle \sigma_i \sigma_{i+a} \rangle$ depending on distance a . Furthermore, let us introduce the dimensionless conformal time coordinate \mathfrak{T} with adapted step size $d\mathfrak{T}/dt = \Gamma e^{-\beta E_B}$ such that

$$\partial_{\mathfrak{T}} c_a = -2c_a + (c_{a+1} + c_{a-1}) \tanh(2\beta J), \quad (8)$$

with the boundary condition $c_{a=0} = 1$.

Setting the left-hand side of Eq. (8) to zero yields the well-known equilibrium solution $c_a = [\tanh(\beta J)]^a$. Note that the 1D Ising model (7) does not have a critical point at finite temperature $T_{\text{crit}} > 0$, instead the analogue of a critical point occurs at zero temperature $T_{\text{crit}} = 0$ where ξ diverges as $\xi \sim e^{2\beta J}$ [23].

In order to understand the non-equilibrium dynamics governed by Eq. (8), let us consider the continuum limit where $c_{a+1} + c_{a-1} - 2c_a$ becomes the second spatial derivative such that we obtain a diffusion-dissipation equation $\partial_{\mathfrak{T}} c = \mathfrak{D} \partial_x^2 c - \gamma c$. For large temperatures, the diffusion coefficient is small $\mathfrak{D} \propto \tanh(2\beta J) \approx 2\beta J \ll 1$ and the damping term $\gamma \approx 2$ dominates. For small temperatures, the damping rate $\gamma = 2 - 2 \tanh(2\beta J)$ is suppressed as $4e^{-4\beta J}$ and the diffusion term $\mathfrak{D} \propto \tanh(2\beta J) \approx 1$ dominates. In analogy to the response time t_{relax} in Eq. (2), we may introduce a response or relaxation time $\mathfrak{T}_{\text{relax}}$ from the inverse damping rate $1/\gamma$ which then scales as $\mathfrak{T}_{\text{relax}} \sim e^{4\beta J}$, i.e., $\mathfrak{T}_{\text{relax}} \sim \xi^2$. Note, however, that the diffusion coefficient stays finite even for $\mathfrak{T}_{\text{relax}} \rightarrow \infty$, i.e., diffusion is still possible.

Freezing in 1D Since analyzing the non-equilibrium dynamics by means of analytic solutions of Eq. (8) is still quite involved, let us consider the weighted sum of correlations $\mathfrak{C} = \sum_{a=1}^{\infty} a c_a$ which obeys the simpler evolution equation

$$\partial_{\mathfrak{T}} \mathfrak{C} = [2 \tanh(2\beta J) - 2] \mathfrak{C} + \tanh(2\beta J). \quad (9)$$

In order to provide an explicit example and to study the analogue of critical slowing down, let us assume the simple cooling protocol $\beta(t) = \kappa t$ (i.e., $T(t) \propto 1/t$) starting at infinite temperature at $t = 0$ and cooling down to zero temperature at $t \rightarrow \infty$. Then this infinite interval of laboratory time $t \in (0, \infty)$ is mapped to a finite interval of conformal time $\mathfrak{T} \in (-\Gamma/[\kappa E_B], 0) = (\mathfrak{T}_{\text{in}}, 0)$.

Incidentally, for our values with $E_B \approx 4J_x$, we may simplify Eq. (9) even further. For low temperatures $\beta J \gg 1$, the source term $\tanh(2\beta J)$ can be approximated by unity and the damping rate γ behaves as $4e^{-4\beta J}$ which for $E_B = 4J$ becomes $4\mathfrak{T}/\mathfrak{T}_{\text{in}}$. As a result, Eq. (9) simplifies to $\partial_{\mathfrak{T}} \mathfrak{C} = -4\mathfrak{C}\mathfrak{T}/\mathfrak{T}_{\text{in}} + 1$. The solution to this equation can be given in terms of the error function, but we may understand its behavior by means of general arguments. In the limit of slow cooling rates considered here, we have $|\mathfrak{T}_{\text{in}}| \gg 1$. Then, starting with $\mathfrak{C} = 0$ at $\mathfrak{T} = \mathfrak{T}_{\text{in}}$, the value of \mathfrak{C} quickly approaches its instantaneous equilibrium value $\mathfrak{C}_{\text{eq}} = \mathfrak{T}_{\text{in}}/(4\mathfrak{T})$. However, once the response time $\mathfrak{T}_{\text{relax}} \sim \mathfrak{T}_{\text{in}}/\mathfrak{T}$ becomes too short $\mathfrak{T}_{\text{relax}} \sim |\mathfrak{T}|$, the system cannot equilibrate anymore and thus the value of \mathfrak{C} freezes in at $\mathfrak{T}_{\text{freeze}} \sim \sqrt{|\mathfrak{T}_{\text{in}}|}$ to its final value $\mathfrak{C}_{\text{freeze}} \sim \sqrt{|\mathfrak{T}_{\text{in}}|}$. Using the asymptotic behavior of the error function, we may also determine the pre-factor to $\mathfrak{C}_{\text{freeze}} = \sqrt{|\mathfrak{T}_{\text{in}}|}/(2\pi)$. Furthermore, as \mathfrak{C} scales with the square of the correlation length ξ_{\parallel} , we

obtain $\xi_{\parallel}^{\text{freeze}} \sim |\mathfrak{T}_{\text{in}}|^{1/4} = (\Gamma/[\kappa E_B])^{1/4}$, which is the analogue to the Kibble-Zurek scaling (3) for this case.

2D Ising model Now we can apply our findings to the anisotropic Ising model (4). Again assuming translational invariance, the evolution equation for the correlations $c_{a,b} = \langle \sigma_{i,j} \sigma_{i+a,j+b} \rangle$ reads

$$\begin{aligned} \partial_{\mathfrak{T}} c_{a,b} = & -2c_{a,b} + (c_{a+1,b} + c_{a-1,b}) \tanh(2\beta J_x) \\ & + \mathcal{O}(J_y, J_x). \end{aligned} \quad (10)$$

Here, we used the separation of scales $J_x, E_B \gg J_y, J_x$ in order to keep the zeroth order in the first line, while all terms which are suppressed by J_y or J_x are in the second line. Note that these terms actually contain factors of $\tanh(2\beta J_y)$ and $\tanh(2\beta J_x)$, i.e., they would not grow without bound even for extremely small temperatures $\beta \sim 1/J_{y,x}$. At such ultra-low temperatures, the rates (6) are exponentially suppressed anyway by the barrier E_B , i.e., basically no flips would occur anymore.

Let us study the behavior resulting from Eq. (10). Since there are no source terms in the first line of Eq. (10) for $b \neq 0$, correlations between rows can only be created by the small terms in the second line, which also contain the source term $c_{0,0} = 1$. Without them, inter-row correlations $c_{a,b \neq 0}$ are only damped or diffused. Since the diffusion in x -direction (i.e., along the rows) is very fast, let us focus on the remaining slower evolution by considering the total correlator between rows $\mathfrak{R}_b = \sum_{a=-\infty}^{\infty} c_{a,b}$

$$\partial_{\mathfrak{T}} \mathfrak{R}_b = [2 \tanh(2\beta J_x) - 2] \mathfrak{R}_b + \mathcal{O}(J_y, J_x), \quad (11)$$

in analogy to Eq. (9). In the following, we consider the total correlation between neighboring rows $b = 1$. In equilibrium, this quantity scales with ξ_{\parallel} , provided that we assume a correlation length ξ_{\perp} of order unity or more. Thus, if ξ_{\parallel} becomes very large, the system would need to shuffle more and more correlations from one row to the next in order to stay close to equilibrium. However, since this can only be done via the small coupling terms $\mathcal{O}(J_y, J_x)$, this bottleneck limits the growth of \mathfrak{R}_b and thus the system departs from equilibrium at some point.

Since this departure time is determined by the smallness of $\mathcal{O}(J_y, J_x)$, the smaller these coupling are, the earlier this departure occurs. Thus, for small $\mathcal{O}(J_y, J_x)$, this departure from equilibrium in the weakly coupled direction will occur earlier than in the strongly coupled direction, where the system can still be close to equilibrium.

Conclusions For a cooling quench of the anisotropic 2D Ising model across the critical point, we studied the freezing of the spatial correlation lengths ξ_{\perp} and ξ_{\parallel} . We found that their dependence on the cooling rate obtained numerically matches the Kibble-Zurek scaling quite well. However, as a distinct signature of the non-equilibrium dynamics in the presence of the anisotropy, we also observed that the ratio $\xi_{\perp}^{\text{freeze}}/\xi_{\parallel}^{\text{freeze}}$ of their frozen values

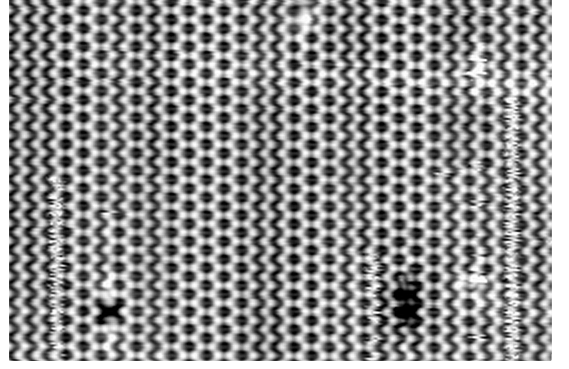


FIG. 3. Low temperature STM image of a Si(001) surface taken at 5 K with $U_{\text{bias}} = 1.3$ V and $I_{\text{tunnel}} = 1$ nA. Field of view is 24×16 nm². Areas with $c(4 \times 2)$ reconstruction exhibit a “honeycomb” pattern. Domain boundaries of the frozen domain structure can be identified by a zig-zag chain of local $p(2 \times 2)$ reconstruction. The two dark spots are missing dimer vacancies and frizzy vertical lines correspond to active phase boundary changes (“phasons”).

differs from the ratio in equilibrium $\xi_{\perp}^{\text{eq}}/\xi_{\parallel}^{\text{eq}}$ by roughly a factor of two. This difference contrasts with the simple picture which underlies the Kibble-Zurek scaling and assumes that the whole system stays close to equilibrium before the freezing time t_{freeze} and basically does not evolve anymore afterwards. Instead, our combination of analytical and numerical methods shows that the non-equilibrium dynamics in the two directions is different and cannot be grasped by a single freezing time t_{freeze} .

Finally, let us discuss potential experimental evidence for the formation of a frozen domain structure for the Si(001) dimerized surface. The surface exhibits parallel rows of alternately buckled dimers which arrange in a $c(4 \times 2)$ reconstruction indicating the anti-phase correlation between neighboring dimer rows [51, 52]. Fig. 3 shows a low-temperature scanning tunneling microscopy image taken at 5 K after preparation of the Si(001) surface through flash annealing and rapid cool-down to liquid nitrogen temperatures $T < 100$ K. The cooling rate was on the order of 1-10 K/s. Further experimental details can be found elsewhere [47]. The STM image was taken at constant current conditions with positive sample bias, i.e., in Fig. 3 filled orbitals of the Si atoms are displayed in bright. The dimer rows run vertically from top to bottom. In each row the alternating buckling along the dimer row can nicely be identified. The anti-phase correlation between neighboring dimers cause the $c(4 \times 2)$ reconstruction which becomes apparent as “honeycomb” pattern. During the rapid cool-down the regime of critical slowing down is reached for $T > T_{\text{crit}}$, resulting in a frozen domain structure which is apparent in Fig. 3. The domain boundaries can be identified as one-dimensional “defects” separating ordered areas with

a $c(4 \times 2)$ reconstruction. As expected from our findings described above and from electron diffraction [36, 37], these ordered domains are extremely elongated. However, albeit quite intriguing, these observations can only be interpreted as a “smoking gun” for the non-equilibrium dynamics studied here and further studies are required to settle this issue.

Acknowledgments Funded by the Deutsche Forschungsgemeinschaft (DFG, German Research Foundation) through the Collaborative Research Center SFB 1242 “Nonequilibrium dynamics of condensed matter in the time domain” (Project-ID 278162697).

-
- [1] P Bak and M Paczuski. Complexity, contingency, and criticality. *PNAS*, 92:6689–6696, 1995.
 - [2] S. L. Sondhi, S. M. Girvin, J. P. Carini, and D. Shahar. Continuous quantum phase transitions. *Rev. Mod. Phys.*, 69:315–333, Jan 1997.
 - [3] Subir Sachdev. *Quantum Phase Transitions*. Cambridge University Press, 2011.
 - [4] T. W. B. Kibble. Topology of cosmic domains and strings. *Journal of Physics A: Mathematical and General*, 9(8):1387, aug 1976.
 - [5] W. H. Zurek. Cosmological experiments in superfluid helium? *Nature*, 317:505–508, 1985.
 - [6] W. H. Zurek, U. Dorner, and P. Zoller. Dynamics of a quantum phase transition. *Physical Review Letters*, 95:105701, 2005.
 - [7] Bogdan Damski. The simplest quantum model supporting the Kibble-Zurek mechanism of topological defect production: Landau-Zener transitions from a new perspective. *Physical Review Letters*, 95:035701, 2005.
 - [8] L. Cincio, J. Dziarmaga, M. M. Rams, and W. H. Zurek. Entropy of entanglement and correlations induced by a quench: Dynamics of a quantum phase transition in the quantum Ising model. *Physical Review A*, 75:052321, 2007.
 - [9] Amit Dutta, R. R. P. Singh, and Uma Divakaran. Quenching through Dirac and semi-Dirac points in optical lattices: Kibble-Zurek scaling for anisotropic quantum critical systems. *Europhysics Letters*, 89(6):67001, apr 2010.
 - [10] Cheng-Wei Liu, Anatoli Polkovnikov, and Anders W. Sandvik. Dynamic scaling at classical phase transitions approached through nonequilibrium quenching. *Phys. Rev. B*, 89:054307, Feb 2014.
 - [11] Paul M. Chesler, Antonio M. García-García, and Hong Liu. Defect formation beyond Kibble-Zurek mechanism and holography. *Phys. Rev. X*, 5:021015, May 2015.
 - [12] Julian Sonner, Adolfo del Campo, and Wojciech H. Zurek. Universal far-from-equilibrium dynamics of a holographic superconductor. *Nature Communications*, 6(1):7406, 2015.
 - [13] Pietro Silvi, Giovanna Morigi, Tommaso Calarco, and Simone Montangero. Crossover from classical to quantum kibble-zurek scaling. *Phys. Rev. Lett.*, 116:225701, Jun 2016.
 - [14] Balázs Dóra, Markus Heyl, and Roderich Moessner. The Kibble-Zurek mechanism at exceptional points. *Nature Communications*, 10:2254, 2019.
 - [15] C.J.O. Reichhardt, A. del Campo, and C. Reichhardt. Kibble-Zurek mechanism for nonequilibrium phase transitions in driven systems with quenched disorder. *Commun Phys*, 5:173, 2022.
 - [16] S. Ulm, J. Roßnagel, G. Jacob, C. Degünther, S. T. Dawkins, U. G. Poschinger, R. Nigmatullin, A. Retzker, M. B. Plenio, F. Schmidt-Kaler, and K. Singer. Observation of the Kibble-Zurek scaling law for defect formation in ion crystals. *Nature Communications*, 4:2290, 2013.
 - [17] Giacomo Lamporesi, Simone Donadello, Simone Serafini, Franco Dalfovo, and Gabriele Ferrari. Spontaneous creation of Kibble-Zurek solitons in a Bose-Einstein condensate. *Nature Physics*, 9:656–660, 2013.
 - [18] Sven Deuschländer, Patrick Dillmann, Georg Maret, and Peter Keim. Kibble-Zurek mechanism in colloidal monolayers. *PNAS*, 112(22):6925–6930, 2015.
 - [19] Jérôme Beugnon and Nir Navon. Exploring the Kibble-Zurek mechanism with homogeneous Bose gases. *Journal of Physics B: Atomic, Molecular and Optical Physics*, 50(2):022002, jan 2017.
 - [20] L.-Y. Qiu, H.-Y. Liang, Y.-B. Yang, H.-X. Yang, T. Tian, Y. Xu, and L.-M. Duan. Observation of generalized Kibble-Zurek mechanism across a first-order quantum phase transition in a spinor condensate. *Science Advances*, 6(21):eaba7292, 2020.
 - [21] Kai Du, Xiaochen Fang, Choongjae Won, Chandan De, Fei-Ting Huang, Wenqian Xu, Hoydoo You, Fernando J. Gómez-Ruiz, Adolfo del Campo, and Sang-Wook Cheong. Kibble-Zurek mechanism of Ising domains. *Nature Physics*, 19:1495–1501, 2023.
 - [22] Barry M. McCoy and Tai Tsun Wu. *The Two-Dimensional Ising Model*. Harvard University Press, Harvard, 1973.
 - [23] Rodney J. Baxter. *Exactly Solved Models in Statistical Mechanics*. Academic Press, London, 1989.
 - [24] Hendrik Hobrecht and Alfred Hucht. Anisotropic scaling of the two-dimensional Ising model I: the torus. *SciPost Phys.*, 7:26, Aug 2019.
 - [25] Hendrik Hobrecht and Alfred Hucht. Anisotropic scaling of the two-dimensional Ising model II: surfaces and boundary fields. *SciPost Phys.*, 8:32, Aug 2020.
 - [26] Alfred Hucht. The square lattice Ising model on the rectangle iii: Hankel and Toeplitz determinants. *Journal of Physics A: Mathematical and Theoretical*, 54(37):375201, sep 2021.
 - [27] Harold J. W. Zandvliet. Phase diagram of the square 2D Ising lattice with nearest neighbor and next-nearest neighbor interactions. *Phase Transitions*, 96(3-4):187–195, 2023.
 - [28] A. Saxena, E.T. Gawlinski, and J.D. Gunton. Structural Phase Transitions on the Si(100) Surface. *Surf. Sci.*, 160(2):618–640, 1985.
 - [29] Masakazu Kubota and Yoshitada Murata. Streak patterns in low-energy electron diffraction on Si(001). *Phys. Rev. B*, 49:4810–4814, Feb 1994.
 - [30] Yoshitada Murata and Masakazu Kubota. Order-disorder transition on Si(001). *Phase Transit.*, 53(2-4):125–141, 1995.
 - [31] K. Inoue, Y. Morikawa, K. Terakura, and M. Nakayama. Order-disorder phase transition on the si(001) surface: Critical role of dimer defects. *Phys. Rev. B*, 49:14774–14777, May 1994.

- [32] Yoshimichi Nakamura, Hiroshi Kawai, and Masatoshi Nakayama. Influence of defects on the order-disorder phase transition of a Si(001) surface. *Phys. Rev. B*, 55:10549–10560, Apr 1997.
- [33] Hiroshi Kawai, Yoshimichi Nakamura, and Masatoshi Nakayama. Kinetic One-Dimensional Ising System on a Narrow Si(001)_{SB} Terrace. *J. Phys. Soc. Jpn.*, 68(12):3936–3940, 1999.
- [34] Devina Pillay, Brett Stewart, Chee Burm Shin, and Gyeong S. Hwang. Revisit to the Ising model for order-disorder phase transition on Si(001). *Surf. Sci.*, 554(2):150–158, 2004.
- [35] Hiroshi Kawai, Osamu Narikiyo, and Kensuke Matsufuji. Structural Phase Transition between $c(4 \times 2)$ and $p(2 \times 2)$ Structures on Si(001) Surface under Observation by Scanning Tunneling Microscopy. *J. Phys. Soc. Jpn.*, 76(3):034602, 2007.
- [36] Christian Brand, Alfred Hucht, Giriraj Jnawali, Jonas D. Fortmann, Björn Sothmann, Hamid Mehdipour, Peter Kratzer, Ralf Schützhold, and Michael Horn-von Hoegen. Dimer coupling energies of the Si(001) surface. *Phys. Rev. Lett.*, 130:126203, Mar 2023.
- [37] Christian Brand, Alfred Hucht, Hamid Mehdipour, Giriraj Jnawali, Jonas D. Fortmann, Mohammad Tajik, Rüdiger Hild, Björn Sothmann, Peter Kratzer, Ralf Schützhold, and Michael Horn von Hoegen. Critical behavior of the dimerized Si(001) surface: A continuous order-disorder phase transition in the 2d Ising universality class. *arXiv:2310.10488*, 2023.
- [38] Lars Onsager. Crystal Statistics. I. A Two-Dimensional Model with an Order-Disorder Transition. *Phys. Rev.*, 65:117–149, Feb 1944.
- [39] J. K. Williams. Monte Carlo estimate of the dynamical critical exponent of the 2D kinetic Ising model. *Journal of Physics A: Mathematical and General*, 18(1):49, jan 1985.
- [40] Nobuyasu Ito, Makoto Taiji, and Masuo Suzuki. Accurate estimation of the dynamical critical exponent of the two-dimensional kinetic Ising model based on the Ising machine m-TIS. *Journal of the Physical Society of Japan*, 56(12):4218–4220, 1987.
- [41] B. Dammann and J. D. Reger. Dynamical critical exponent of the two-dimensional Ising model. *Europhysics Letters*, 21(2):157, jan 1993.
- [42] Christian Munkel, Dieter W. Heermann, Joan Adler, Misha Gofman, and Dietrich Stauffer. The dynamical critical exponent of the two-, three- and five-dimensional kinetic Ising model. *Physica A: Statistical Mechanics and its Applications*, 193(3):540–552, 1993.
- [43] M. P. Nightingale and H. W. J. Blöte. Dynamic exponent of the two-dimensional Ising model and Monte Carlo computation of the subdominant eigenvalue of the stochastic matrix. *Phys. Rev. Lett.*, 76:4548–4551, Jun 1996.
- [44] B. C. S. Grandi and W. Figueiredo. Dynamical critical exponent of a nonequilibrium Ising model. *Phys. Rev. E*, 54:4722–4725, Nov 1996.
- [45] M. P. Nightingale and H. W. J. Blöte. Monte Carlo computation of correlation times of independent relaxation modes at criticality. *Phys. Rev. B*, 62:1089–1101, Jul 2000.
- [46] J. Dąbrowski, E. Pehlke, and M. Scheffler. Calculation of the surface stress anisotropy for the buckled si(001)(1×2) and $p(2 \times 2)$ surfaces. *Phys. Rev. B*, 49:4790–4793, Feb 1994.
- [47] Y. Pennec, M. Horn-von Hoegen, Xiaobin Zhu, D. C. Fortin, and M. R. Freeman. Dynamics of an Ising Chain under Local Excitation: A Scanning Tunneling Microscopy Study of Si(100) Dimer Rows at 5 K. *Phys. Rev. Lett.*, 96:026102, Jan 2006.
- [48] F. M. Bulnes, V. D. Pereyra, and J. L. Riccardo. Collective surface diffusion: n -fold way kinetic Monte Carlo simulation. *Phys. Rev. E*, 58:86–92, Jul 1998.
- [49] Kurt Binder and Dieter W. Heermann. *Rejection-Free Monte Carlo*, pages 179–190. Springer International Publishing, Cham, 2019.
- [50] Peter Kratzer. *Multiscale Simulation Methods in Molecular Sciences*, volume 42 of *NIC Series*, chapter Monte Carlo and Kinetic Monte Carlo Methods – A Tutorial, pages 51–76. John von Neumann Institute for Computing (NIC), Jülich Supercomputing Centre, Forschungszentrum Jülich, 52425 Jülich, Germany, 2009.
- [51] Robert A. Wolkow. Direct observation of an increase in buckled dimers on Si(001) at low temperature. *Phys. Rev. Lett.*, 68(17):2636, 1992.
- [52] R. G. Zhao and W. S. Yang. Atomic structure of the Si(001) $c(4 \times 2)$ surface. *Phys. Rev. B*, 33(10):6780, 1986.
- [53] Roy J. Glauber. Time-dependent statistics of the Ising model. *Journal of Mathematical Physics*, 4(2):294–307, 12 1963.
- [54] Yuji Sakai and Koji Hukushima. Dynamics of one-dimensional Ising model without detailed balance condition. *Journal of the Physical Society of Japan*, 82(6):064003, 2013.

Appendix: 1D Ising model

A closer look at the Glauber-Arrhenius rates (6) shows that for the energy differences arising for a single-spin flip at site i in the 1D Ising model

$$E_{\sigma} - E_{\sigma'} = 2J\sigma_i(\sigma_{i-1} + \sigma_{i+1}), \quad (12)$$

the rates can be represented by a quadratic function of the spins near that site [53, 54] with

$$\frac{1}{e^{\beta(E_{\sigma} - E_{\sigma'})} + 1} = \frac{1}{2} - \frac{\tanh(2\beta J)}{4} \sigma_i(\sigma_{i-1} + \sigma_{i+1}), \quad (13)$$

which with $\sigma_i^2 = 1$ enables to convert the rate equations (5) into exact evolution equations for the non-equilibrium expectation values

$$\partial_t \langle \sigma_i \rangle = \Gamma e^{-\beta E_B} \left[\tanh(2\beta J) \frac{\langle \sigma_{i+1} \rangle + \langle \sigma_{i-1} \rangle}{2} - \langle \sigma_i \rangle \right] \quad (14)$$

and similarly for the two-point functions

$$\begin{aligned} \partial_t \langle \sigma_i \sigma_j \rangle = \Gamma e^{-\beta E_B} & \left[-2 \langle \sigma_i \sigma_j \rangle + \tanh(2\beta J) \times \right. \\ & \left. \times \frac{\langle \sigma_{i+1} \sigma_j \rangle + \langle \sigma_{i-1} \sigma_j \rangle + \langle \sigma_i \sigma_{j+1} \rangle + \langle \sigma_i \sigma_{j-1} \rangle}{2} \right]. \quad (15) \end{aligned}$$

If we start in the symmetric phase $\langle \sigma_i \rangle = 0$, the mean field $\langle \sigma_i \rangle$ in Eq. (14) stays zero as expected. However, due to $\langle \sigma_i \sigma_i \rangle = \langle \sigma_i^2 \rangle = 1$, the evolution equation (15) for the correlations contains a source term and thus correlations are generated even if they are absent initially.

Appendix: 2D Ising model

For the anisotropic 2D Ising model – compare Eq. (4) with $J_x \rightarrow J_{\parallel}$, $J_y \rightarrow J_{\perp}$, and $J_{\times} \rightarrow 0$ – the energy difference upon flipping a single spin at site (i, j) is

$$E_{\sigma} - E_{\sigma'} = 2J_{\parallel} \sigma_{ij} (\sigma_{i-1,j} + \sigma_{i+1,j}) + 2J_{\perp} \sigma_{ij} (\sigma_{i,j-1} + \sigma_{i,j+1}), \quad (16)$$

such that the Glauber rates (6) lead to a quartic representation

$$\begin{aligned} \frac{1}{e^{\beta(E_{\sigma} - E_{\sigma'})} + 1} &= \frac{1}{2} - f_x \sigma_{ij} (\sigma_{i-1,j} + \sigma_{i+1,j}) \\ &\quad - f_y \sigma_{ij} (\sigma_{i,j-1} + \sigma_{i,j+1}) \\ &\quad + g_x \sigma_{ij} (\sigma_{i-1,j} + \sigma_{i+1,j}) \sigma_{i,j-1} \sigma_{i,j+1} \\ &\quad + g_y \sigma_{ij} \sigma_{i-1,j} \sigma_{i+1,j} (\sigma_{i,j-1} + \sigma_{i,j+1}), \end{aligned} \quad (17)$$

with the abbreviations

$$\begin{aligned} f_x &= \frac{[1 + 2 \cosh(4\beta J_{\parallel}) + \cosh(4\beta J_{\perp})] \tanh(2\beta J_{\parallel})}{16 \cosh(2\beta J_{\parallel} + 2\beta J_{\perp}) \cosh(2\beta J_{\parallel} - 2\beta J_{\perp})}, \\ f_y &= \frac{[1 + 2 \cosh(4\beta J_{\perp}) + \cosh(4\beta J_{\parallel})] \tanh(2\beta J_{\perp})}{16 \cosh(2\beta J_{\parallel} + 2\beta J_{\perp}) \cosh(2\beta J_{\parallel} - 2\beta J_{\perp})}, \\ g_x &= \frac{\sinh^2(2\beta J_{\perp}) \tanh(2\beta J_{\parallel})}{4 \cosh(4\beta J_{\parallel}) + 4 \cosh(4\beta J_{\perp})}, \\ g_y &= \frac{\sinh^2(2\beta J_{\parallel}) \tanh(2\beta J_{\perp})}{4 \cosh(4\beta J_{\parallel}) + 4 \cosh(4\beta J_{\perp})}, \end{aligned} \quad (18)$$

which shows that will in general not be possible to obtain exact closed evolution equations, as first-order terms will couple to third-order correlators, second-order correlators couple to fourth-order terms and so on. This hierarchy of correlators can however be closed at some order by mean-field-type approximations, leading in general to nonlinear equations.

If we would keep only two-point correlators and neglect all three-point and higher correlations, the above equation (10) would again become a diffusion-dissipation equation (in the continuum limit), but with an anisotropic diffusion kernel. The damping term γ would then vanish at the critical temperature T_{crit} of the 2D Ising model (4). However, while the restriction to two-point correlations is exact for the 1D Ising model, it is only an approximation for the 2D case. Moreover, this approximation is expected to become quite inaccurate near the critical point.